Crystal Structure of the RIM2 C_2A-Domain at 1.4 Å Resolution[†,‡]

Han Dai,[§,||] Diana R. Tomchick,[§] Jesús García,[§,||,⊥] Thomas C. Südhof,[@] Mischa Machius,[§] and Josep Rizo*[,§,||]

Department of Biochemistry, Department of Pharmacology, Center for Basic Neuroscience, Department of Molecular Genetics, and Howard Hughes Medical Institute, University of Texas Southwestern Medical Center, 5323 Harry Hines Boulevard, Dallas, Texas 75390

Received July 13, 2005; Revised Manuscript Received August 15, 2005

ABSTRACT: RIMs are large proteins that contain two C_2-domains and are localized at presynaptic active zones, where neurotransmitters are released. RIMs play key roles in synaptic vesicle priming and regulation of presynaptic plasticity. A mutation in the RIM1 C_2A-domain has been implicated in autosomal dominant cone−rod dystrophy (CORD7). The RIM C_2A-domain does not contain the full complement of aspartate residues that commonly mediate Ca^{2+} binding at the top loops of C_2-domains, and has been reported to interact with SNAP-25 and synaptotagmin 1, two proteins from the Ca^{2+}-dependent membrane fusion machinery. Here we have used NMR spectroscopy and X-ray crystallography to analyze the structure and biochemical properties of the RIM2 C_2A-domain, which is closely related to the RIM1 C_2A-domain. We find that the RIM2 C_2A-domain does not bind Ca^{2+}. Moreover, little binding of the RIM2 C_2A-domain to SNAP-25 and to the C_2-domains of synaptotagmin 1 was detected by NMR experiments, suggesting that as yet unidentified interactions of the RIM C_2A-domain mediate its function. The crystal structure of the RIM2 C_2A-domain using data to 1.4 Å resolution reveals a β-sandwich that resembles those observed for other C_2-domains, but exhibits a unique dipolar distribution of electrostatic charges whereby one edge of the β-sandwich is highly positive and the other edge is highly negative. The location of the mutation site implicated in CORD7 at the bottom of the domain and the pattern of sequence conservation suggest that, in contrast to most C_2-domains, the RIM C_2A-domains may function through Ca^{2+}-independent interactions involving their bottom face.

The release of neurotransmitters by Ca^{2+}-triggered synaptic vesicle exocytosis is a central event in interneuronal communication. This process is highly regulated and involves several steps, which include docking of the synaptic vesicles to the presynaptic plasma membrane, one or more priming reactions that leave the vesicles in a release-ready state, and the actual Ca^{2+}-evoked release of neurotransmitters when an action potential reaches the presynaptic terminal (*1*). Release is restricted to specialized sites of the presynaptic plasma membrane known as active zones. The different steps that lead to exocytosis are controlled by a complex protein machinery. This machinery is formed in part by components that have homologues in all types of intracellular membrane traffic such as the SNARE proteins synaptobrevin, syntaxin, and SNAP-25,[1] which play a key role in membrane fusion, and Rab3s, which are small GTPases that regulate neurotransmitter release (reviewed in refs *2* and *3*). In addition, neurotransmitter release is controlled by specialized proteins such as the Ca^{2+} sensor synaptotagmin 1 (reviewed in refs *4* and *5*) and the components of the active zone, among others.

Active zones integrate presynaptic signals that regulate neurotransmitter release and are formed by a network of large proteins, which include RIMs, Munc13s, Bassoon, piccolo, ELKS, and liprins (reviewed in ref *6*). Among these proteins, RIMs are particularly interesting because of the multiple roles in regulating release and organizing the active zone that have been suggested by genetic and biochemical experiments. RIMs were initially identified as Rab3 effectors (*7*) and include four genes in mammals (*RIM1*, *RIM2*, *RIM3*γ, and *RIM4*γ) (*8*) and one in *Caenorhabditis elegans* (*unc10*) (*9*). The mammalian *RIM1* and *RIM2* genes specify full-length transcripts encoding two closely related protein products (RIM1α and RIM2α, respectively) that contain an N-terminal zinc finger domain, a PDZ domain, and two C-terminal C_2-domains (called C_2A-domain and C_2B-domain). In addition, the *RIM2* gene specifies a shorter transcript lacking the N-terminal zinc finger (*RIM2*β) and an even shorter transcript (*RIM2*γ) that, like *RIM3*γ and *RIM4*γ, only encodes the C_2B-domain and adjacent sequences (*8*). Unc10 mutants in *C. elegans* exhibit a drastic decrease in the level of release that is associated with a defect in synaptic vesicle priming (*9*). Deletion of RIM1α in mice leads to a milder phenotype, probably because of redundancy with RIM2α, but still results in less vesicle priming and alteration of short-term synaptic

[†] This work was supported by NIH Grant NS40944 to J.R.

[‡] Structures have been deposited in the Protein Data Bank (entry 2bwq).

* To whom correspondence should be addressed. Phone: (214) 645-6360. Fax: (214) 645-6353. E-mail: jose@arnie.swmed.edu.

[§] Department of Biochemistry.

[||] Department of Pharmacology.

[⊥] Current address: RMN de Biomolecules, Parc Cientific de Barcelona, Barcelona, Spain.

[@] Center for Basic Neuroscience, Department of Molecular Genetics, and Howard Hughes Medical Institute.

[1] Abbreviations: CORD7, autosomal dominant cone−rod dystrophy; HSQC, heteronuclear single-quantum correlation; LTP, long-term potentiation; PDB, Protein Data Bank; PKC, protein kinase C; RIM, Rab3-interacting molecule; RIM-BP, RIM binding protein; SNAP-25, synaptosomal-associated protein of 25 kDa.

10.1021/bi0513608 CCC: $30.25
Published on Web 09/23/2005

plasticity (*10*, *11*). Moreover, a form of long-term synaptic plasticity known as mossy fiber LTP is completely abolished in these mice (*12*). RIM1α knockout mice exhibit severe defects in memory and learning (*13*) that most likely arise from these defects in neurotransmitter release and its regulation.

The different domains of α-RIMs have been implicated in multiple protein−protein interactions. Thus, the N-terminal zinc finger domain and adjacent regions are involved in binding to Rab3s (*7*) and to Munc13-1 (*14*), an active zone protein with a key role in synaptic vesicle priming, while the PDZ domain binds to ELKS (also known as ERC or CAST) (*15*). On the other hand, the RIM C_2A-domain was reported to bind to synaptotagmin 1 and to SNAP-25 (*16*), whereas the C_2B-domain was also found to bind to synaptotagmin 1 and in addition to liprins (*10*). Finally, a proline-rich sequence between the two C_2-domains binds to RIM-binding proteins (RIM-BPs) (*17*). These observations suggest that α-RIMs may act as scaffolds that help to organize the active zone through its multiple interactions with active zone proteins, and at the same time may regulate neurotransmitter release by binding to key components of the release apparatus. However, some of the biochemical studies that described these interactions relied largely on GST pull-down experiments, which are prone to artifacts (*18*); for instance, no binding of synaptotagmin 1 to the RIM2 C_2A-domain was observed in GST pull-down experiments performed in a separate study (*10*). Moreover, little is know about the three-dimensional structures of the α-RIM domains. Due in part to this scarcity of structural and definitive biochemical information, there is currently a large gap between the extensive genetic and physiological data describing the functions of α-RIMs and the limited molecular understanding of these functions.

In this study, we have focused on the structure and interactions of the RIM C2A-domain. This domain plays a critical role in the proper localization of *unc10* in *C. elegans* (*19*), and its functional importance was emphasized by the observation that an R844H point mutation in the RIM1α C_2A-domain segregates with autosomal dominant cone−rod dystrophy (CORD7) (*20*). However, the RIM C_2A-domain is only distantly related to the C_2-domains that have been more thoroughly studied, and it is unclear to what extent it shares their properties. C_2-domains are widespread protein modules that usually bind phospholipids in a Ca^{2+}-dependent manner and have a β-sandwich structure with loops emerging at the top and bottom of the sandwich (reviewed in ref *21*). Multiple Ca^{2+} ions commonly bind to a motif formed by five conserved aspartate residues located at the top loops (*22*−*25*), which also mediate phospholipid binding (*26*, *27*). However, some C_2-domains do not bind Ca^{2+} or phospholipids. The RIM C_2A-domain does not contain the full complement of aspartate residues that form the C_2-domain Ca^{2+}-binding motif. This observation suggests that the RIM C_2A-domain does not bind Ca^{2+}, but this prediction has not been tested. Moreover, because of the limited degree of sequence identity with C_2-domains of known three-dimensional structure, it is unknown whether the RIM C_2A-domain contains specific structural features that may be critical for its function.

To shed light on these questions and provide a structural basis for understanding the role(s) of the C_2A-domain from RIMs, we have analyzed the biochemical properties of the RIM2 C_2A-domain using NMR spectroscopy, and we have determined its crystal structure using data to 1.4 Å resolution. We find that the RIM2 C_2A-domain does not bind to Ca^{2+}, phospholipids, synaptotagmin 1, or SNAP-25 with significant affinity, suggesting that other interactions mediate its function. The RIM2 C_2A-domain adopts a β-sandwich structure that resembles those of other C_2-domains such as the C_2A-domain of synaptotagmin 1, but exhibits a striking dipolar distribution of electrostatic potential, with a highly positive potential on one edge of the β-sandwich and a highly negative potential at the opposite edge. The location of the conserved arginine side chain implicated in CORD7 at the bottom of the domain and the pattern of sequence conservation in RIM C_2A-domains suggest that these domains may function through Ca^{2+}-independent interactions mediated by its bottom face, in contrast to the common involvement of Ca^{2+}-dependent interactions of the top loops in C_2-domain function.

EXPERIMENTAL PROCEDURES

Sample Preparation. DNA encoding GST fusion proteins of various fragments spanning the rat RIM2 C_2A-domain were made using custom-designed primers and standard PCR cloning techniques and subcloned into the pGEX-KG expression vector. The R805H RIM2 C_2A-domain point mutant (residues 722−859) was generated by site-directed mutagenesis (Stratagene) according to the manufacturer's protocol. The fusion proteins were expressed at 25 °C in *Escherichia coli* BL21 and isolated by affinity chromatography on glutathione-Sepharose followed by on-resin cleavage with thrombin. The eluted proteins were further purified by gel-filtration chromatography on a S75 column (Amersham). Uniform ^{15}N labeling was achieved by growing the bacteria in $^{15}NH_4Cl$ as the sole nitrogen source.

NMR Spectroscopy. All NMR experiments were carried out at 27 °C on Varian INOVA500 or INOVA600 spectrometers with samples containing approximately 100 μM C_2-domains dissolved in 20 mM MES (pH 6.0) and 150 mM NaCl. Ca^{2+} titrations monitored by $^1H-^{15}N$ HSQC experiments were performed as described previously (*25*). All the NMR binding experiments were carried out at 27 °C on Varian INOVA500 or INOVA600 spectrometers with samples containing 60 μM ^{15}N-labeled proteins and 80 μM nonlabeled proteins dissolved in 20 mM MES (pH 6.0) and 150 mM NaCl in the presence or absence of 10 mM $CaCl_2$. All NMR data were processed with NMRPipe (*28*) and analyzed with NMRView (*29*).

X-ray Crystallography. Rat RIM2 C_2A-domain (residues 722−859) dissolved in 20 mM MES (pH 6.0), 150 mM NaCl, and 1 mM EDTA was concentrated to 25 mg/mL and crystallized in 17.5% (w/v) PEG 4000, 0.2 M $(NH_4)_2SO_4$, and 0.1 M sodium acetate (pH 4.5) at 20 °C using the hanging-drop vapor-diffusion method. Crystals appeared overnight and grew to a final size of 0.05 mm × 0.05 mm × 0.1 mm within 2 days. Prior to data collection, crystals were transferred into a solution of 20% (w/v) PEG 4000, 0.15 M NaCl, 0.2 M $(NH_4)_2SO_4$, 0.1 M sodium acetate (pH 4.5), and 15% (v/v) ethylene glycol, and then flash-cooled in liquid propane. Diffraction data were collected at Structural Biology Center beamlines 19BM and 19ID of the Advanced

Table 1: Data Collection and Refinement Statistics[a]

data collection	
space group	$P2_1$
unit cell dimensions	
a, *b*, *c* (Å)	25.45, 44.81, 55.76
β (deg)	103.86
resolution (Å)	20.92−1.41 (1.43−1.41)[b]
completeness	98.5 (82.0)[b]
R_{merge}[c] (%)	2.2 (18.3)[b]
$I/\sigma(I)$	52.9 (5.2)[b]
multiplicity	4.0 (2.8)[b]
Wilson *B* value (Å^2)	15.98
refinement	
resolution (Å)	20.00−1.41
no. of reflections R_{work}/R_{free}	21884/1383
R_{work}/R_{free} (%)	18.10/21.35
no. of solvent molecules	104
no. of sulfate ions	2
average *B* value (Å^2)	17.74
rmsd for bond lengths (Å)	0.019
rmsd for bond angles (deg)	1.92

[a] Data collection values are as defined in the program HKL2000. [b] Values in parentheses are for the highest-resolution shell. [c] $R_{merge} = 100\sum_h\sum_i|I_{h,i} - \langle I_h\rangle|/\sum_h\sum_i I_{h,i}$, where the outer sum (*h*) is over the unique reflections and the inner sum (*i*) is over the set of independent observations of each unique reflection.

Photon Source at 100 K to a Bragg spacing (d_{min}) of ~1.41 Å. The crystals exhibited the symmetry of space group $P2_1$, contained one molecule per asymmetric unit, and had the following unit cell parameters: $a = 25.45$ Å, $b = 44.81$ Å, $c = 55.76$ Å, and $\beta = 103.86°$. Data were processed and scaled in the HKL2000 program suite (*30*). The rat RIM2 C_2A-domain structure was determined via molecular replacement using AMoRe (*31*). Initial model coordinates were obtained by modifying the coordinates of the human RIM2 C_2A-domain (PDB entry 1v27). The rotation and translation function search was conducted with data between a d_{min} of 8.0 and 4.0 Å, and a single solution was obtained with a final correlation coefficient of 0.50. Model refinement was carried out with Refmac (*32*) of the CCP4 package (*33*) with a random subset of all data set aside for the calculation of R_{free}. Manual adjustments to the models were carried out with O (*34*). The electron density clearly showed the presence of two sulfate ions. After refinement of the protein part was complete, solvent molecules were added where stereochemically reasonable. The model has good stereochemistry, with 87.7% of residues in the most favored region of the Ramachandran plot and none in disallowed regions. Data collection and refinement statistics are listed in Table 1.

RESULTS

Definition of Domain Boundaries and Biochemical Analysis. The region of RIM2 that contains the predicted C_2A-domain exhibits only a limited degree of sequence similarity with C_2-domains of known structure, particularly at the C-terminus where C_2-domains tend to be more variable. For instance, the synaptotagmin 1 C_2B-domain contains two C-terminal α-helices that are not present in the synaptotagmin 1 C_2A-domain and, as a result, is 20 residues longer (*18*, *22*). To experimentally define the correct boundaries of the RIM2 C_2A-domain, we expressed several constructs spanning residues 662−869 of RIM2, performed limited proteolysis experiments with trypsin and chymotrypsin, and identified proteolytically resistant fragments by mass spectrometry (data not shown). On the basis of these experiments, we focused on a minimal fragment containing residues 722−859 of RIM2. A ^{1}H−^{15}N HSQC spectrum of a uniformly ^{15}N-labeled sample of this fragment in the absence of Ca^{2+} (Figure 1, black contours) revealed an excellent chemical shift dispersion, demonstrating that the fragment is properly folded and thus contains the RIM2 C_2A-domain. All experiments described below were performed with this fragment, which hereafter we will call the RIM2 C_2A-domain for simplicity.

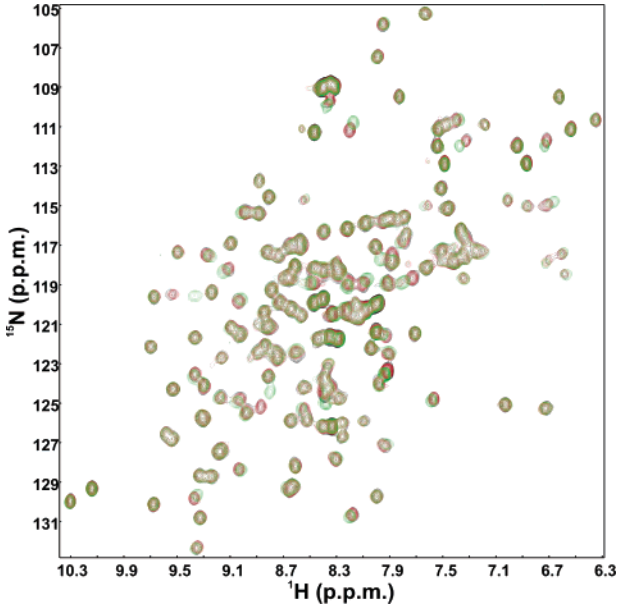

FIGURE 1: RIM2 C_2A-domain does not bind Ca^{2+}. ^{1}H−^{15}N HSQC spectra of the RIM2 C_2A-domain in the absence (black contours) and presence of 1 mM Ca^{2+} (red contours) or 20 mM Ca^{2+} (green contours) are shown.

In addition to providing information about the proper folding of a protein, ^{1}H−^{15}N HSQC spectra are also useful in analyzing interactions of a ^{15}N-labeled protein in solution. ^{1}H−^{15}N HSQC spectra contain one cross-peak for the amide group of each non-proline residue in the protein. The positions of the cross-peaks are very sensitive to the chemical environment of the amide groups. Hence, perturbations in these cross-peaks (shifts or broadening) report on interactions with ligands or other proteins. To analyze whether the RIM2 C_2A-domain binds Ca^{2+}, we acquired additional ^{1}H−^{15}N HSQC spectra in the presence of 1 and 20 mM Ca^{2+} (Figure 1, red and green contours, respectively). Addition of 1 mM Ca^{2+} did not induce significant perturbations, showing that the RIM2 C_2A-domain does not bind Ca^{2+} at this concentration. A few cross-peaks exhibited small shifts in the presence of 20 mM Ca^{2+}. This behavior is characteristic of C_2-domains that do not bind Ca^{2+} with significant affinity and can be attributed to weak binding of Ca^{2+} to oxygen-rich clusters at the surface of a protein (*35*, *36*). We also investigated whether the RIM2 C_2A-domain binds negatively charged phospholipids using a fluorescence resonance energy transfer-based assay (*18*), but we did not observe any significant binding in the absence or presence of Ca^{2+} (data not shown).

The interactions of the RIM C_2A-domain with SNAP-25 and synaptotagmin 1 were identified using pull-down experiments with GST fusion proteins immobilized on GST affinity resins (*16*). However, GST pull-down experiments are prone to artifacts that can yield false positive or negative results. For instance, we previously described that immobilized GST

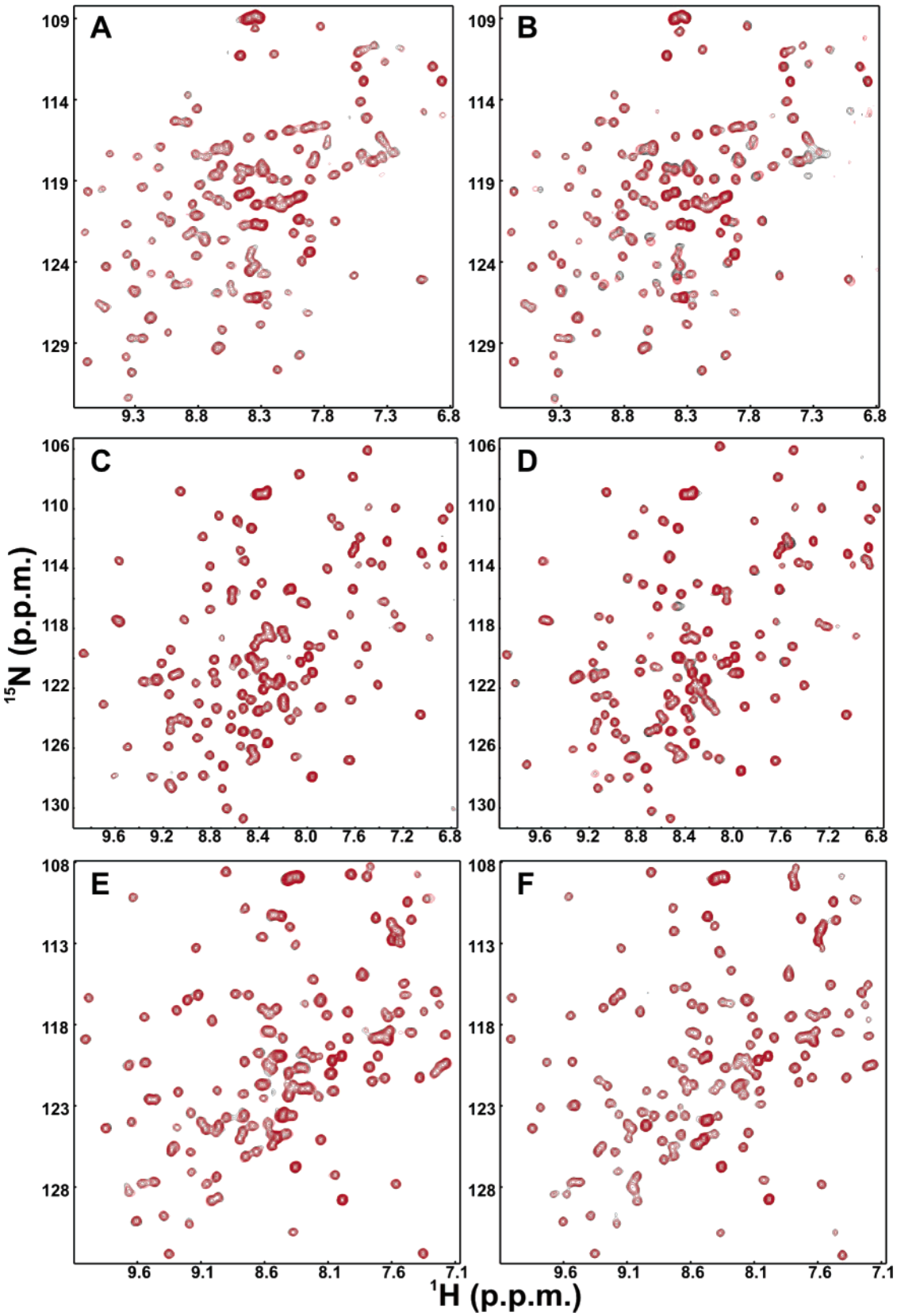

FIGURE 2: RIM2 C_2A-domain does not bind to SNAP-25 and the synaptotagmin 1 C_2-domains. (A and B) $^{1}H-^{15}N$ HSQC spectra of the RIM2 C_2A-domain before (black) and after (red) addition of unlabeled SNAP-25 in the absence (A) and presence (B) of 10 mM Ca^{2+}. (C−F) $^{1}H-^{15}N$ HSQC spectra of the synaptotagmin 1 C_2A-domain (C and D) and C_2B-domain (E and F) before (black) and after (red) addition of the unlabeled RIM2 C_2A-domain in the absence (C and E) or presence (D and F) of 10 mM Ca^{2+}.

fusions of the synaptotagmin 1 C_2B-domain have a strong tendency to bind to polyacidic compounds that are very difficult to remove even with extensive washes of the resins and that can induce artifactual binding or mask relevant interactions (*37*). To test whether the RIM2 C_2A-domain binds to SNAP-25 and synaptotagmin 1 by an independent

method, we used NMR spectroscopy. Addition of unlabeled SNAP-25 did not cause significant perturbation of the $^1H-^{15}N$ HSQC spectrum of the ^{15}N-labeled RIM2 C_2A-domain in the absence of Ca^{2+} (Figure 2A), showing that the RIM2 C_2A-domain and SNAP-25 do not interact under these conditions. Only minor spectral changes were observed in analogous experiments performed in the presence of 10 mM Ca^{2+} (Figure 2B). These minor changes may reflect a very low affinity interaction that is likely to be nonspecific and that contrasts with the nanomolar affinity observed in GST pull-down experiments (*16*). To test for interactions between the RIM2 C_2A-domain and synaptotagmin 1, we prepared ^{15}N-labeled samples of the synaptotagmin 1 C_2A-domain and C_2B-domain and recorded the effects that addition of the unlabeled RIM2 C_2A-domain has on their $^1H-^{15}N$ HSQC spectra in the absence and presence of 10 mM Ca^{2+} (Figure 2C−F). The RIM2 C_2A-domain did not cause any significant perturbations in these spectra, showing that it does not bind to the synaptotagmin 1 C_2-domains. It should be noted that these experiments were performed in solution with purified fragments that do not contain any tags (such as GST) and that have been extensively characterized by NMR spectroscopy. In addition, these experiments were performed at protein concentrations of 60−80 μM that favor the formation of protein complexes even if they have low affinity. Hence, we conclude that the RIM2 C_2A-domain does not form binary complexes with SNAP-25 and the synaptotagmin 1 C_2-domains either in the presence or absence of Ca^{2+} with significant affinity.

Three-Dimensional Structure of the RIM2 C_2A-Domain at 1.4 Å Resolution. To investigate whether the RIM2 C_2A-domain has specific structural features, we turned to X-ray crystallography. Crystals of the RIM2 C_2A-domain grew overnight in 17.5% (w/v) PEG 4000, 0.2 M $(NH_4)_2SO_4$, and 0.1 M sodium acetate (pH 4.5) at 20 °C. The structure was determined by molecular replacement using as a search model an NMR structure of the human RIM2 C_2A-domain that was deposited in the PDB (entry 1v27) as part of a structural genomics initiative, but has not been described in the literature. The crystal structure was refined using data to 1.4 Å resolution. A ribbon diagram of the RIM2 C_2A-domain is shown in Figure 3, and the structural statistics are summarized in Table 1. A portion of the electron density is shown in Figure 4A. Like other C_2-domains, the structure of the RIM2 C_2A-domain consists of a β-sandwich formed by two four-stranded β-sheets. The bottom of the domain contains a short 3_{10}-helix in the loop connecting strands 5 and 6, which often contains a short α-helix in other C_2-domains, too. No electron density was observed for the loop connecting strands 6 and 7, which is usually called loop 3 and is commonly involved in binding of Ca^{2+} to C_2-domains (*21*). This loop is ordered in most C_2-domains whose structures have been elucidated, but it is highly charged and somewhat longer in the RIM2 C_2A-domain, which likely results in its greater flexibility.

Two prominent, tetrahedrally shaped electron density peaks that can be attributed to sulfate ions are observed near the bottom loop of the RIM2 C_2A-domain that contains the 3_{10}-helix (Figure 4A). One sulfate ion interacts with the backbone amide nitrogens of R805 and R806, two nitrogens from the guanidine group of the R806 side chain, and two water molecules. The other sulfate ion is also bound to the

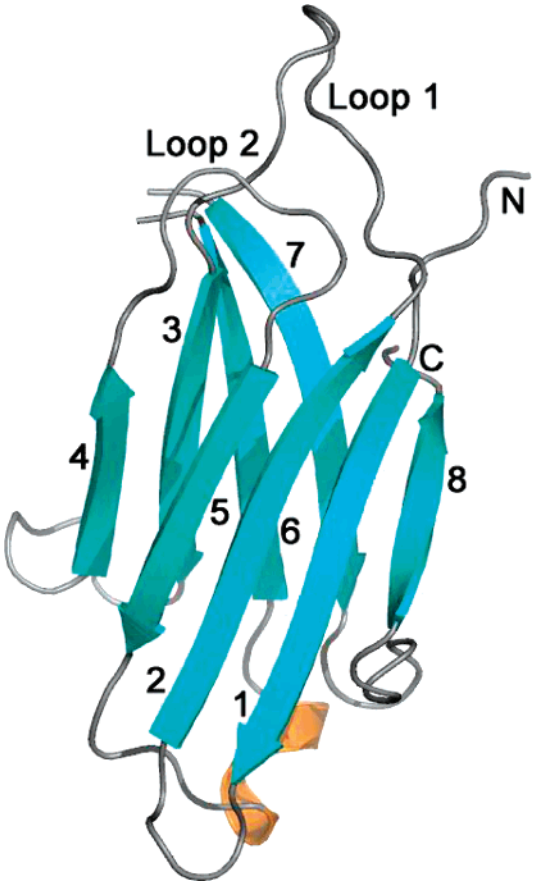

FIGURE 3: Ribbon diagram of the rat RIM2 C_2A-domain. The β-strands are colored in cyan and labeled from 1 to 8. The 3_{10}-helix is colored orange. The canonical Ca^{2+}-binding loops are labeled loop 1 and loop 2 (loop 3 is disordered). N and C indicate the N- and C-termini, respectively. This figure was prepared with Insight II (MSI, San Diego, CA) and Molscript (*47*).

guanidine side chain group of R806 and is coordinated by an additional water molecule. Figure 4B shows a ribbon-and-stick diagram illustrating the relative orientations of the side chains in this region, which includes the R805 side chain. This side chain is in a position equivalent to R844 of the human RIM1α C_2A-domain, which has been identified as a mutation site (to His) in CORD7 patients (*20*). The exposed nature of this side chain suggests that the Arg to His mutation does not affect folding of the domain, which we confirmed with the observation that the $^1H-^{15}N$ HSQC spectrum of the ^{15}N-labeled R805H mutant RIM2 C_2A-domain is similar to that of the wild-type RIM2 C_2A-domain and exhibits only minor perturbations (data not shown). Thus, it is most likely that the mutation causes disease by interfering with an interaction(s) of the RIM C_2A-domain with a target molecule. The observation of the two bound sulfate ions in the crystal structure of the RIM2 C_2A-domain, which might mimic the negative charges of a target, also suggests that this region may act as an interaction site through its multiple positively charged residues.

The potential importance of electrostatic forces for the interactions of the RIM C_2A-domain was further emphasized by examination of its surface electrostatic potential. Intriguingly, this analysis revealed a striking dipolar distribution, with a highly positively charged surface on the edge of the β-sandwich that includes the 3_{10}-helix region at the bottom, and a highly negatively charged surface on the opposite edge

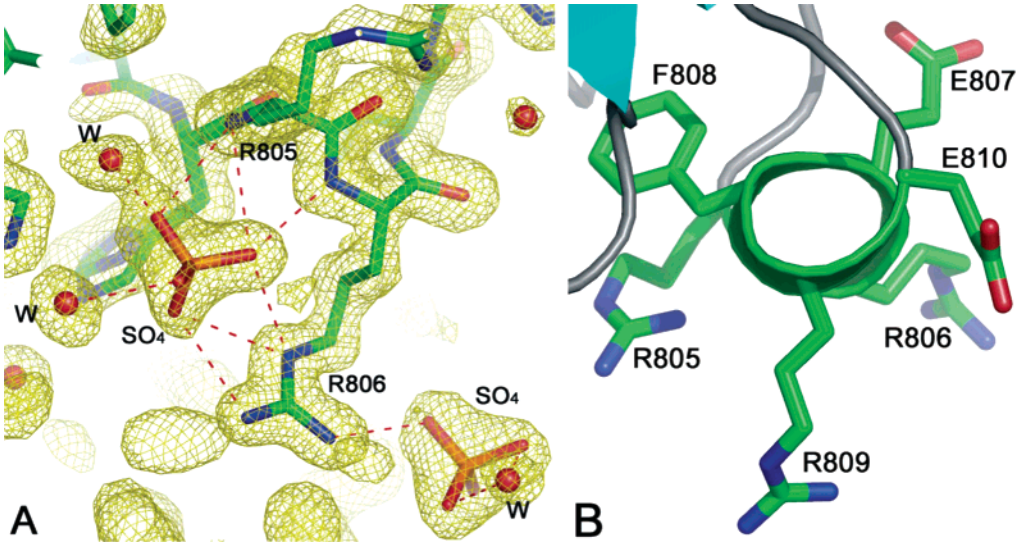

FIGURE 4: Binding of sulfate ions to a positively charged region at the bottom of the RIM2 C_2A-domain. (A) A $2F_o - F_c$ electron density map contoured at 1σ of the bottom loop of the rat RIM2 C_2A-domain where two sulfate ions bind. Oxygen atoms are colored red, nitrogen atoms blue, sulfur atoms orange, and carbon atoms green. Water molecules hydrogen bonded to the two sulfate ions are labeled W. This figure was prepared using PyMol (DeLano Scientific, San Carlos, CA). (B) Ribbon-and-stick representation of the bottom 3_{10}-helix viewed along the helix axis.

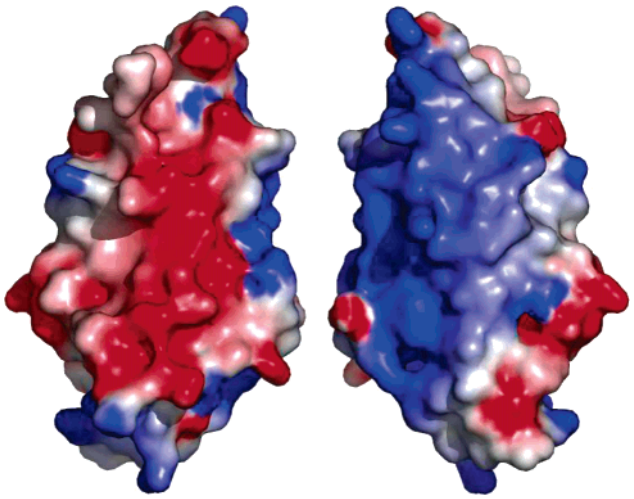

FIGURE 5: RIM2 C_2A-domain with a dipolar distribution of electrostatic charges. Two views of the electrostatic surface potential of the rat RIM2 C_2A-domain rotated 180° with respect to the vertical axis are shown. In the left panel, strands 7 and 8 are in the front, while in the right panel, strands 4 and 5 are in the front. Hydrogen atoms were generated using CNS (*48*), and the electrostatic surface potential was computed with GRASP (*49*) and rendered with PyMol. The electrostatic potential is contoured at the 5 kT/e level, with red denoting negative potential and blue denoting positive potential.

(Figure 5). The positively charged edge is formed by strands 4 and 5, and its highly positive potential is due in part to the abundance of basic residues in strand 4. The opposite edge of the β-sandwich is formed by strands 7 and 8, both of which contain negatively charged residues. Overall, the basic and acidic residues that lead to the dipolar character of the RIM C_2A-domain are generally conserved in RIM C_2A-domains (Figure 6). Correspondingly, analysis of the surface electrostatic potential in models of the RIM C_2A-domains from different species, built by homology with the structure of the rat RIM C_2A-domain, also revealed a dipolar charge distribution, although this dipolar character is less pronounced in the unc10 C_2A-domain because of a lower degree of conservation of the charged residues (data not shown).

Comparison of the RIM C_2A-Domains with Other C_2-Domains. C_2-domains usually form β-sandwiches that can have two different topologies resulting from a circular permutation of the β-strands (called topology I and II) (*21*, *38*). The structure of the RIM C_2A-domain conforms to topology I, which is also observed in other C_2-domains involved in intracellular membrane traffic such as those from synaptotagmins (*18*, *22*, *35*, *39*, *40*) and rabphilin (*41*), as well as in some C_2-domains involved in signal transduction such as those of PKCs (*42*, *43*). A structural comparison performed with DALI (*44*) revealed that, as expected, the RIM2 C_2A-domain is closely structurally similar to other C_2-domains. The highest *Z* score yielded by DALI in the search (18.2) corresponds to the crystal structure of the synaptotagmin 1 C_2A-domain (*22*), which exhibits a trace rms deviation of 1.7 Å for 119 equivalent Cα atoms with respect to the RIM2 C_2A-domain. A trace superposition of the synaptotagmin 1 and RIM2 C_2A-domains (Figure 7A) shows that there is a remarkable similarity between the two structures in the β-sheets, and that differences occur largely at a few loops connecting the β-strands, particularly at the C-terminal loop connecting strands 7 and 8. Indeed, ribbon superpositions of the known C_2-domain structures revealed that the conformation of this loop is highly variable in C_2-domains, as illustrated with the RIM2 C_2A-domain, the synaptotagmin 1 C_2A-domain and C_2B-domain, and the PKC-β C_2-domain in Figure 7B. Note that some degree of diversity is observed in the structure of most loops, and in some cases, they can diverge considerably [e.g., the cPLA$_2$ C_2-domain contains an α-helix inserted in loop 1 (*45*)]. However, the high variability of the loop connecting strands 7 and 8 in basically all C_2-domains is particularly pronounced.

The alignment shown in Figure 6 compares the sequences of the RIM C_2A-domains from different species together with those of the rat RIM C_2B-domain and of other rat C_2-domains

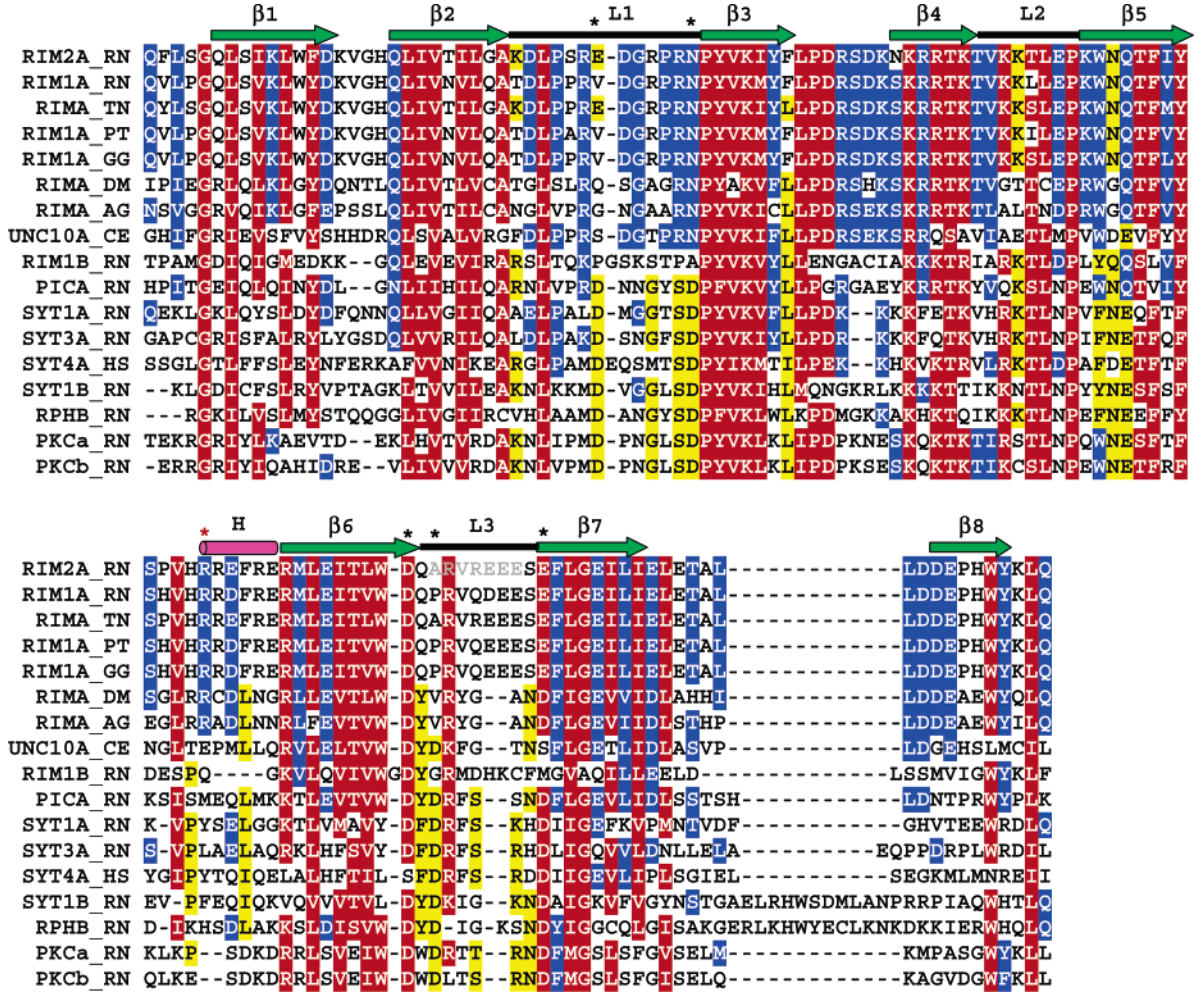

FIGURE 6: Sequence alignment of the RIM C_2A-domains from different species and selected rat C_2-domains. Residues conserved in most C_2-domains (>80% of the sequences displayed; E = D, K = R, N = Q, L = V = I = M, F = Y, and S = T) are colored white with a red background. Residues that appear to be selectively conserved in RIM C_2A-domains are colored white with a blue background. Residues that appear to be selectively conserved in other C_2-domains, but not in RIM C_2A-domains, are colored black with a yellow background. Residues invisible in the rat RIM2 C2A-domain structure are colored gray. The secondary structure elements of the rat RIM2 C2A-domain are shown at the top of the alignment. The three top loops that are usually involved in binding of Ca^{2+} to C_2-domains, the 3_{10}-helix, and the β-strands are represented by black bars, a magenta cylinder, and green arrows, respectively. The black asterisks indicate the positions of the five aspartate residues that are commonly involved in binding of Ca^{2+} to C_2-domains. The red asterisk indicates the position corresponding to the mutation site involved in CORD7. Piccolo, synaptotagmin, and rabphilin are abbreviated PIC, SYT, and RPH, respectively. A and B at the end of the protein name refers to the C_2A-domain and the C_2B-domain, respectively. Species abbreviations: RN, rat (*Rattus norvegicus*); HS, human (*Homo sapiens*); PT, chimpanzees (*Pan troglodytes*); GG, chicken (*Gallus gallus*); TN, spotted green puffer fish (*Tetraodon nigroviridis*); DM, fruit fly (*Drosophila melanogaster*); AG, Mosquito (*Anopheles gambiae*); and CE, round worm (*C. elegans*). GenBank entries Q9JIS1 for RIM2A_RN, Q9JIR4 for RIM1A_RN, CAF98072 for RIMA_TN, XP_527433 for RIM1A_PT, XP_419884 for RIM1A_GG, AAF55479 for RIMA_DM, XP_321402 for RIMA_AG, Q22366 for UNC10A_CE, Q9JIR4 for RIM1B_RN, NP_064483 for PICA_RN, P21707 for SYT1A_RN, NP_061995 for SYT3A_RN, AAH36538 for SYT4A_HS, P21707 for SYT1B_RN, NP_598202 for RPHB_RN, XP_343976 for PKCa_RN, and NP_036845 for PKCb_RN.

with type I topology. The alignment illustrates that the C-terminal sequences of C_2-domains are in general more variable than the remaining sequences, particularly in the region connecting strands 7 and 8. This observation correlates with the structural diversity in this region. However, it is noteworthy that this region exhibits a relatively high degree of conservation in RIMs, and is included among several regions that are conserved in RIMs but differ in other C_2-domains (highlighted in blue in Figure 6; note that these regions may still be conserved in different species for a given C_2-domain). Interestingly, the strand 7−strand 8 region contains several acidic residues that are selectively conserved in RIM C_2A-domains and that contribute to their dipolar character. Strand 4 and adjacent sequences, which also contribute substantially to this dipolar character, contain several basic residues that are selectively conserved in RIM C_2A-domains. However, this region is basic in most C_2-domains, particularly in the synaptotagmin 1 C_2B-domain (*18*), and thus includes basic residues that are conserved throughout the C_2-domain family (highlighted in red in Figure 6). Overall, these observations suggest that the striking dipolar nature is a unique property of the RIM C_2A-domains. A survey of the surface electrostatic potential of several C_2-domains revealed that some degree of charge separation is actually observed in several of them, although it is generally not as marked as in the RIM2 C_2A-domain (Figure 1 of the Supporting Information).

It is also worth noting that loop 3 at the top of the domain, which usually contains three of the aspartate side chains that coordinate Ca^{2+} in Ca^{2+}-dependent C_2-domains (*23*) and is

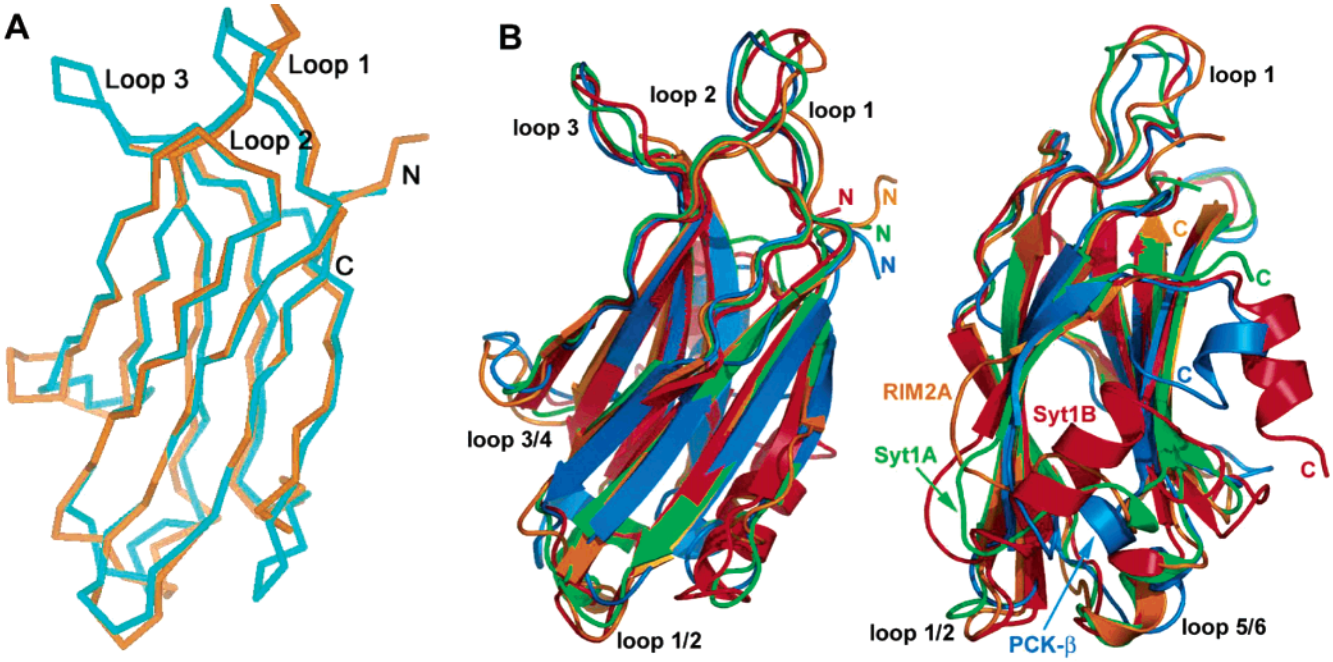

FIGURE 7: Comparison of the structures of the RIM2 C_2A-domain and other C_2-domains. (A) Trace superposition of the RIM2 C_2A-domain (orange) and the synaptotagmin 1 C_2A-domain (cyan). (B) Two different views of ribbon superpositions of the RIM2 C_2A-domain (orange), the synaptotagmin 1 C_2A-domain (green) and C_2B-domain (red), and the PKC-β C_2-domain (blue). The positions of the top loops commonly implicated in Ca^{2+} binding, as well as the N- and C-termini, are indicated in panels A and B. In panel B, the positions of the loops connecting strands 1 and 2, strands 3 and 4, and strands 5 and 6 are labeled as loop 1/2, loop 3/4, and loop 5/6, respectively, and the position of the loop connecting strands 7 and 8 is indicated with the color-coded name of the protein.

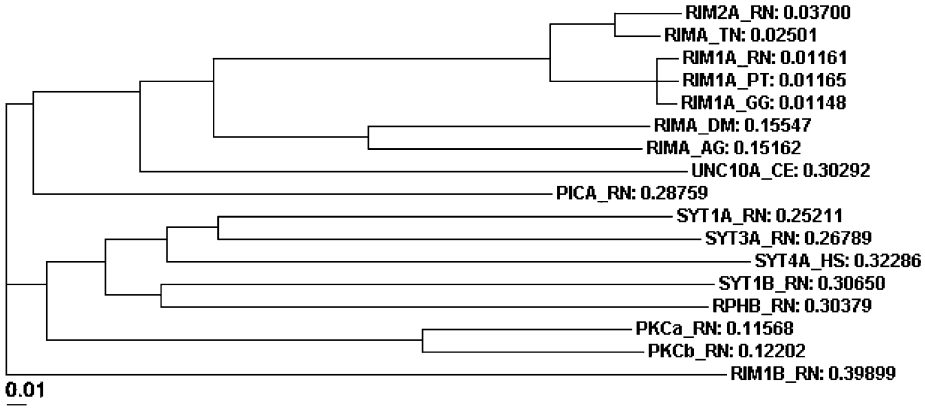

FIGURE 8: Phylogram tree of RIM C_2A-domains from different species and selected rat C_2-domains. The tree was generated with CLUSTAL W (*50*) using the sequence alignment of Figure 6. The branch lengths are proportional to the inferred evolutionary change. The scores given at the right reflect the inferred evolutionary change from the closest branch point.

directly involved in phospholipid binding (*26*, *27*), exhibits a relatively low level of sequence conservation in RIM C_2A-domains. This contrasts with the high level of conservation of residues in the strand 3−strand 4 and strand 7−strand 8 regions at the bottom half of the domain, which also contains the R805 residue that is mutated in RIM1α of CORD7 patients. These observations suggest that the bottom part of the RIM C_2A-domains may play a key role in their function, in contrast to the preponderant role that the top half plays in Ca^{2+}-dependent C_2-domains.

The differences between the RIM C_2A-domains and the C_2-domains from synaptotagmins, rabphilin, and PKCs are emphasized in the dendogram shown in Figure 8, which was constructed on the basis of the sequence alignment of Figure 6. The dendogram shows that the synaptotagmin, rabphilin, and PKC C_2-domains are more closely related to each other than to the RIM C_2A-domains. This finding does not correlate strictly with the inability of the RIM C_2A-domains to bind Ca^{2+}, since the synaptotagmin 4 C_2A-domain is also unable to bind Ca^{2+} (*35*). In addition, the piccolo C_2A-domain binds Ca^{2+} (*46*) but is more closely related to the RIM C_2A-domains than to the synaptotagmin, rabphilin, and PKC C_2-domains (Figure 8). The rat RIM C_2B-domain, which is also predicted to be unable to bind Ca^{2+}, appears to be equally distant from the RIM C_2A-domains and the synaptotagmin, rabphilin, and PKC C_2-domains.

DISCUSSION

RIMs are large, multidomain proteins of the presynaptic active zone that play key roles in synaptic vesicle priming and regulation of short- and long-term presynaptic plasticity (*9*−*12*). These multiple roles are most likely associated with interactions of RIMs with target molecules. Indeed, multiple interactions of the RIM domains with active zone proteins

and with proteins implicated in Ca^{2+}-dependent membrane fusion have been described (*7*, *10*, *14*−*17*), suggesting that RIMs help to organize the active zone and regulate neurotransmitter release by directly influencing the membrane fusion apparatus. However, there is little information about the nature and the relevance of these interactions, as well as about the three-dimensional structures of the RIM domains. This scarcity of structural and biochemical information hinders the development of a molecular understanding of the functions of RIMs, which on the other hand have been extensively characterized by genetic and physiological experiments.

To help develop such an understanding, in this work we have focused on the structure and interactions of the RIM2 C_2A-domain. We find that this domain does not bind Ca^{2+}, as predicted on the basis of the observation that the RIM2 C_2A-domain does not contain the full complement of aspartate residues that form the canonical C_2-domain Ca^{2+}-binding motif (see Figure 6). In addition, our data reveal no significant binding of the RIM2 C_2A-domain to SNAP-25 and to the synaptotagmin 1 C_2-domains either in the presence or in the absence of Ca^{2+}. Binding of the RIM C_2A-domain to SNAP-25 and synaptotagmin 1 had been previously investigated using pull-down assays with immobilized GST fusion proteins (*16*). These experiments were motivated by the observation that the RIM C_2A-domain contains multiple basic residues in strand 4, which are also present in the synaptotagmin 1 C_2B-domain and were implicated in its oligomerization as well as in interactions with other targets. However, this polybasic region of the synaptotagmin 1 C_2B-domain was shown to bind avidly to polyacidic compounds such as DNA and RNA, which are very difficult to remove from immobilized GST fusion proteins and could induce artifactual interactions (*37*). For instance, the purified synaptotagmin 1 C_2B-domain was shown to be monomeric in solution (*37*). Thus, it seems likely that interactions of the RIM C_2A-domain with synaptotagmin 1 and SNAP-25 observed with GST pull-down experiments (*16*), which we could not confirm with our NMR experiments, may arise from incomplete removal of acidic contaminants in the immobilized proteins. Indeed, mutations in the polybasic region of the RIM C_2A-domain abolished binding to synaptotagmin 1 (*16*), consistent with this proposal. Our NMR data cannot rule out the possibility that the RIM C_2A-domain interacts with synaptotagmin 1 sequences outside its C_2-domains, but it should be noted that no interaction between the RIM C_2A-domain and synaptotagmin 1 from brain extracts was observed in separate GST pull-down experiments (*10*). On the basis of the crucial importance of the RIM C_2A-domain for proper localization (*19*), it is tempting to speculate that an as yet unidentified interaction with another active zone protein may underlie the primary function of the RIM C_2A-domain.

The crystal structure of the RIM2 C_2A-domain and the comparison with other C_2-domains described here further emphasize the pattern of conservation and divergence that has been emerging from structural studies of these intriguing protein modules. On one hand, the similarity between the structures of the RIM2 C_2A-domain and the synaptotagmin 1 C_2A-domain (Figure 7A) shows the high degree of structural conservation of the core of the β-sandwich. On the other hand, this and other structural comparisons between C_2-domains (e.g., Figure 7B) illustrate the variability in the loops connecting the strands of the β-sandwich, which thus appears to act as a scaffold for diverse sequences emerging at the top and the bottom. Particularly striking is the diversity of the loop connecting strands 7 and 8 at the bottom of the domain. While the significance of this diversity remains to be established, the functional importance of the bottom of the RIM C_2A-domain is supported by the selective conservation of several residues in the strand 7−strand 8 region of the RIM C_2A-domain, and by the implication of the RIM1α R844H mutation in CORD7. A key functional role for the bottom of the RIM C_2A-domains would represent a new paradigm for the range of mechanisms of action of C_2-domains, which until now have been largely shown to function through the Ca^{2+}-dependent interactions mediated by their top loops. A distinct mechanism of action for the RIM C_2A-domains would not be surprising given the observation that the C_2-domains of synaptotagmins, rabphilins, and PKCs are more closely related to each other than to the RIM C_2A-domains (Figure 8). The finding that the RIM2 C_2A-domain exhibits an unusual dipolar distribution of electrostatic charges that is conserved in most RIM C_2A-domains suggests that this dipolar character may be critical for its role in neurotransmitter release. In particular, the presence of a highly positively charged surface that includes the arginine mutated in CORD7 patients suggests that an interaction of the RIM C_2A-domain with a highly acidic target may be crucial for its function. Further research will be needed to test these ideas and identify which interaction(s) mediates the function of the RIM C_2A-domain. The crystal structure of the RIM2 C_2A-domain described here provides a framework for understanding the basis of this function.

ACKNOWLEDGMENT

Use of the Argonne National Laboratory Structural Biology Center beamlines at the Advanced Photon Source was supported by the U.S. Department of Energy, Office of Biological and Environmental Research, under Contract W-31-109-ENG-38.

SUPPORTING INFORMATION AVAILABLE

Gallery of the electrostatic surface potential of different C_2A-domains. This material is available free of charge via the Internet at http://pubs.acs.org.

REFERENCES

1. Sudhof, T. C. (1995) The synaptic vesicle cycle: A cascade of protein−protein interactions, *Nature 375*, 645−653.
2. Lin, R. C., and Scheller, R. H. (2000) Mechanisms of synaptic vesicle exocytosis, *Annu. Rev. Cell Dev. Biol. 16*, 19−49.
3. Rizo, J., and Sudhof, T. C. (2002) Snares and munc18 in synaptic vesicle fusion, *Nat. Rev. Neurosci. 3*, 641−653.
4. Sudhof, T. C. (2002) Synaptotagmins: Why so many? *J. Biol. Chem. 277*, 7629−7632.
5. Tucker, W. C., and Chapman, E. R. (2002) Role of synaptotagmin in Ca^{2+}-triggered exocytosis, *Biochem. J. 366*, 1−13.
6. Garner, C. C., Kindler, S., and Gundelfinger, E. D. (2000) Molecular determinants of presynaptic active zones, *Curr. Opin. Neurobiol. 10*, 321−327.
7. Wang, Y., Okamoto, M., Schmitz, F., Hofmann, K., and Sudhof, T. C. (1997) Rim is a putative Rab3 effector in regulating synaptic-vesicle fusion, *Nature 388*, 593−598.

8. Wang, Y., and Sudhof, T. C. (2003) Genomic definition of RIM proteins: Evolutionary amplification of a family of synaptic regulatory proteins, *Genomics 81*, 126−137.
9. Koushika, S. P., Richmond, J. E., Hadwiger, G., Weimer, R. M., Jorgensen, E. M., and Nonet, M. L. (2001) A post-docking role for active zone protein Rim, *Nat. Neurosci. 4*, 997−1005.
10. Schoch, S., Castillo, P. E., Jo, T., Mukherjee, K., Geppert, M., Wang, Y., Schmitz, F., Malenka, R. C., and Sudhof, T. C. (2002) RIM1α forms a protein scaffold for regulating neurotransmitter release at the active zone, *Nature 415*, 321−326.
11. Calakos, N., Schoch, S., Sudhof, T. C., and Malenka, R. C. (2004) Multiple roles for the active zone protein RIM1α in late stages of neurotransmitter release, *Neuron 42*, 889−896.
12. Castillo, P. E., Schoch, S., Schmitz, F., Sudhof, T. C., and Malenka, R. C. (2002) RIM1α is required for presynaptic long-term potentiation, *Nature 415*, 327−330.
13. Powell, C. M., Schoch, S., Monteggia, L., Barrot, M., Matos, M. F., Feldmann, N., Sudhof, T. C., and Nestler, E. J. (2004) The presynaptic active zone protein RIM1α is critical for normal learning and memory, *Neuron 42*, 143−153.
14. Betz, A., Thakur, P., Junge, H. J., Ashery, U., Rhee, J. S., Scheuss, V., Rosenmund, C., Rettig, J., and Brose, N. (2001) Functional interaction of the active zone proteins Munc13-1 and RIM1 in synaptic vesicle priming, *Neuron 30*, 183−196.
15. Wang, Y., Liu, X. R., Biederer, T., and Sudhof, T. C. (2002) A family of RIM-binding proteins regulated by alternative splicing: Implications for the genesis of synaptic active zones, *Proc. Natl. Acad. Sci. U.S.A. 99*, 14464−14469.
16. Coppola, T., Magnin-Luthi, S., Perret-Menoud, V., Gattesco, S., Schiavo, G., and Regazzi, R. (2001) Direct interaction of the Rab3 effector RIM with Ca^{2+} channels, SNAP-25, and synaptotagmin, *J. Biol. Chem. 276*, 32756−32762.
17. Wang, Y., Sugita, S., and Sudhof, T. C. (2000) The RIM/NIM family of neuronal C2 domain proteins. Interactions with Rab3 and a new class of Src homology 3 domain proteins, *J. Biol. Chem. 275*, 20033−20044.
18. Fernandez, I., Arac, D., Ubach, J., Gerber, S. H., Shin, O., Gao, Y., Anderson, R. G., Sudhof, T. C., and Rizo, J. (2001) Three-dimensional structure of the synaptotagmin 1 c_2b-domain. Synaptotagmin 1 as a phospholipid binding machine, *Neuron 32*, 1057−1069.
19. Deken, S. L., Vincent, R., Hadwiger, G., Liu, Q., Wang, Z. W., and Nonet, M. L. (2005) Redundant localization mechanisms of RIM and ELKS in *Caenorhabditis elegans*, *J. Neurosci. 25*, 5975−5983.
20. Johnson, S., Halford, S., Morris, A. G., Patel, R. J., Wilkie, S. E., Hardcastle, A. J., Moore, A. T., Zhang, K., and Hunt, D. M. (2003) Genomic organisation and alternative splicing of human RIM1, a gene implicated in autosomal dominant cone-rod dystrophy (CORD7), *Genomics 81*, 304−314.
21. Rizo, J., and Sudhof, T. C. (1998) C2-domains, structure and function of a universal Ca^{2+}-binding domain, *J. Biol. Chem. 273*, 15879−15882.
22. Sutton, R. B., Davletov, B. A., Berghuis, A. M., Sudhof, T. C., and Sprang, S. R. (1995) Structure of the first C2 domain of synaptotagmin I: A novel Ca^{2+}/phospholipid-binding fold, *Cell 80*, 929−938.
23. Shao, X., Davletov, B. A., Sutton, R. B., Sudhof, T. C., and Rizo, J. (1996) Bipartite Ca^{2+}-binding motif in C2 domains of synaptotagmin and protein kinase C, *Science 273*, 248−251.
24. Essen, L. O., Perisic, O., Lynch, D. E., Katan, M., and Williams, R. L. (1997) A ternary metal binding site in the C2 domain of phosphoinositide-specific phospholipase C-δ1, *Biochemistry 36*, 2753−2762.
25. Ubach, J., Zhang, X., Shao, X., Sudhof, T. C., and Rizo, J. (1998) Ca^{2+} binding to synaptotagmin: How many Ca^{2+} ions bind to the tip of a C2-domain? *EMBO J. 17*, 3921−3930.
26. Zhang, X., Rizo, J., and Sudhof, T. C. (1998) Mechanism of phospholipid binding by the C2A-domain of synaptotagmin I, *Biochemistry 37*, 12395−12403.
27. Chapman, E. R., and Davis, A. F. (1998) Direct interaction of a Ca^{2+}-binding loop of synaptotagmin with lipid bilayers, *J. Biol. Chem. 273*, 13995−14001.
28. Delaglio, F., Grzesiek, S., Vuister, G. W., Zhu, G., Pfeifer, J., and Bax, A. (1995) Nmrpipe: A Multidimensional Spectral Processing System Based on Unix Pipes, *J. Biomol. NMR 6*, 277−293.
29. Johnson, B. A., and Blevins, R. A. (1994) NMR View: A Computer-Program for the Visualization and Analysis of NMR Data, *J. Biomol. NMR 4*, 603−614.
30. Otwinowski, Z., and Minor, W. (1997) Processing of X-ray diffraction data collected in oscillation mode, *Macromol. Crystallogr. A276*, 307−326.
31. Navaza, J. (1994) Amore: An Automated Package for Molecular Replacement, *Acta Crystallogr. A50*, 157−163.
32. Murshudov, G. N., Vagin, A. A., and Dodson, E. J. (1997) Refinement of macromolecular structures by the maximum-likelihood method, *Acta Crystallogr. D53*, 240−255.
33. Bailey, S. (1994) The Ccp4 Suite: Programs for Protein Crystallography, *Acta Crystallogr. D50*, 760−763.
34. Jones, T. A., Zou, J. Y., Cowan, S. W., and Kjeldgaard, M. (1991) Improved Methods for Building Protein Models in Electron-Density Maps and the Location of Errors in These Models, *Acta Crystallogr. A47*, 110−119.
35. Dai, H., Shin, O. H., Machius, M., Tomchick, D. R., Sudhof, T. C., and Rizo, J. (2004) Structural basis for the evolutionary inactivation of Ca^{2+} binding to synaptotagmin 4, *Nat. Struct. Mol. Biol. 11*, 844−849.
36. Chen, X., Tang, J., Sudhof, T. C., and Rizo, J. (2005) Are neuronal SNARE proteins Ca^{2+} sensors? *J. Mol. Biol. 347*, 145−158.
37. Ubach, J., Lao, Y., Fernandez, I., Arac, D., Sudhof, T. C., and Rizo, J. (2001) The C2B domain of synaptotagmin I is a Ca^{2+}-binding module, *Biochemistry 40*, 5854−5860.
38. Nalefski, E. A., and Falke, J. J. (1996) The C2 domain calcium-binding motif: Structural and functional diversity, *Protein Sci. 5*, 2375−2390.
39. Shao, X., Fernandez, I., Sudhof, T. C., and Rizo, J. (1998) Solution structures of the Ca^{2+}-free and Ca^{2+}-bound C2A domain of synaptotagmin I: Does Ca^{2+} induce a conformational change? *Biochemistry 37*, 16106−16115.
40. Sutton, R. B., Ernst, J. A., and Brunger, A. T. (1999) Crystal structure of the cytosolic C2A−C2B domains of synaptotagmin III. Implications for Ca^{2+}-independent snare complex interaction, *J. Cell Biol. 147*, 589−598.
41. Ubach, J., Garcia, J., Nittler, M. P., Sudhof, T. C., and Rizo, J. (1999) Structure of the Janus-faced C2B domain of rabphilin, *Nat. Cell Biol. 1*, 106−112.
42. Sutton, R. B., and Sprang, S. R. (1998) Structure of the protein kinase Cβ phospholipid-binding C2 domain complexed with Ca^{2+}, *Structure 6*, 1395−1405.
43. Verdaguer, N., Corbalan-Garcia, S., Ochoa, W. F., Fita, I., and Gomez-Fernandez, J. C. (1999) Ca^{2+} bridges the C2 membrane-binding domain of protein kinase Cα directly to phosphatidylserine, *EMBO J. 18*, 6329−6338.
44. Holm, L., and Sander, C. (1993) Protein structure comparison by alignment of distance matrices, *J. Mol. Biol. 233*, 123−138.
45. Perisic, O., Fong, S., Lynch, D. E., Bycroft, M., and Williams, R. L. (1998) Crystal structure of a calcium-phospholipid binding domain from cytosolic phospholipase A2, *J. Biol. Chem. 273*, 1596−1604.
46. Garcia, J., Gerber, S. H., Sugita, S., Sudhof, T. C., and Rizo, J. (2004) A conformational switch in the Piccolo C2A domain regulated by alternative splicing, *Nat. Struct. Mol. Biol. 11*, 45−53.
47. Kraulis, P. J. (1991) Molscript: A Program to Produce Both Detailed and Schematic Plots of Protein Structures, *J. Appl. Crystallogr. 24*, 946−950.
48. Brunger, A. T., Adams, P. D., Clore, G. M., DeLano, W. L., Gros, P., Grosse-Kunstleve, R. W., Jiang, J. S., Kuszewski, J., Nilges, M., Pannu, N. S., Read, R. J., Rice, L. M., Simonson, T., and Warren, G. L. (1998) Crystallography & NMR system: A new software suite for macromolecular structure determination, *Acta Crystallogr. D54* (Part 5), 905−921.
49. Nicholls, A., Sharp, K. A., and Honig, B. (1991) Protein Folding and Association: Insights from the Interfacial and Thermodynamic Properties of Hydrocarbons, *Proteins: Struct., Funct., Genet. 11*, 281−296.
50. Higgins, D., Thompson, J., Gibson, T., Thompson, J. D., Higgins, D. G., and Gibson, T. J. (1994) CLUSTAL W: Improving the sensitivity of progressive multiple sequence alignment through sequence weighting, position-specific gap penalties and weight matrix choice, *Nucleic Acids Res. 22*, 4673−4680.

BI0513608